IEEE Open Journal of Vehicular Technology

Received 13 June 2023; accepted 18 June 2023. Date of publication 20 June 2023;
date of current version 5 July 2023. The review of this article was coordinated by Editor S. Guo.

Digital Object Identifier 10.1109/OJVT.2023.3288041

Heterogeneous In-Band Full-Duplex System for Simultaneous SUN-FSK Transmission and SUN-OFDM Reception

YUDAI MORIKAWA, KEIICHI MIZUTANI (Member, IEEE), AND HIROSHI HARADA (Member, IEEE)

Kyoto University, Kyoto 606-8501, Japan

CORRESPONDING AUTHOR: HIROSHI HARADA (e-mail: hiroshi.harada@i.kyoto-u.ac.jp).

This work was supported by the Ministry of Internal Affairs and Communications (MIC) in Japan under Grant JPJ000254.

ABSTRACT This study proposes a heterogeneous in-band full-duplex system for the simultaneous transmission of the existing wireless smart ubiquitous network (Wi-SUN) using IEEE 802.15.4g-compliant frequency-shift keying for smart utility network (SUN-FSK) and reception of the next-generation Wi-SUN using IEEE 802.15.4-2020-compliant orthogonal frequency-division multiplexing for SUN (SUN-OFDM). In particular, we propose a digital self-interference (SI) cancellation scheme based on high-precision SI channel estimation using the moving average method, which can be used when the SI signal is a SUN-FSK signal and the desired signal is a SUN-OFDM signal. Furthermore, we propose a highly efficient SUN-OFDM demodulation technique that considers the effect of residual SI. We evaluate the proposed methods through computer simulations. The proposed methods can achieve 67 dB of SI cancellation in the digital domain when the SI signal power and desired signal power ratio in the digital domain is 50 dB. The results of this study enable more efficient coexistence of the existing and next-generation Wi-SUNs, which is expected to improve the throughput and responsiveness of next-generation Wi-SUN systems employing SUN-OFDM.

INDEX TERMS Channel estimation, in-band full duplex, self-interference cancellation, SUN-FSK, SUN-OFDM, Wi-SUN.

I. INTRODUCTION

The Internet of things (IoT) is a key enabling technology for smart cities, industries, and agriculture. Various IoT projects are underway in many countries [1], and the number of connected IoT devices is expected to reach 14.7 billion by 2023 [2]. Currently, IoT systems are enabled by numerous wireless solutions, such as wireless fidelity (Wi-Fi) [3], ZigBee [4], long-range wide area network (LoRaWAN) [5], Sigfox [6], and wireless smart ubiquitous network (Wi-SUN) [7]. Wireless solutions for IoT systems should be characterized by low cost, flexible network construction, long-distance communication, high data rate (approximately several hundred kbit/s), and massive-node connectivity [8]. The wireless solution should be based on international standards to achieve low cost. When the solution is based on international standards, vendors can develop devices based on common specifications, enabling a stable supply of devices in the long term. Wi-Fi and ZigBee were developed based on international standards (IEEE 802.11 [9] and IEEE 802.15.4, respectively [10]); however, they have numerous limitations for use in IoT systems, such as the difficulty in accommodating massive terminals, coverage area, installation cost, and power consumption [11]. Thus, the use of Wi-SUN has increased globally, particularly in the United States and Japan [12].

Wi-SUN is a standard developed by the Wi-SUN alliance based on IEEE 802.15.4. It achieves low power consumption by adopting IEEE 802.15.4g-compliant filtered frequency-shift keying (filtered-FSK) for the physical layer [13], [14], [15], supports multi-hop relaying to provide wide coverage [16], [17], and achieves a data rate of 50–400 kbit/s that is relatively high, regarding the wireless solutions for the IoT [13]. In IEEE 802.15.4, the filtered-FSK for a smart utility network (SUN) is called SUN-FSK [10]. Wi-SUN is used in most energy meters (that is, smart meters) in Japan and the foundation of various IoT networks. Recently, Wi-SUN systems have been required to support IoT networks with higher

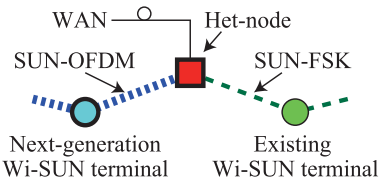

FIGURE 1. Coexistence of the SUN-FSK-based existing and SUN-OFDM-based next-generation Wi-SUN terminals in the same frequency channel.

data rates, real-time transmission, and terminal mobility (e.g., connected car systems). The adoption of a physical layer capable of more than 600 kbit/s is being considered [18], [19], [20]. In particular, IEEE 802.15.4-2020-compliant orthogonal frequency-division multiplexing for SUN (SUN-OFDM) is promising because it can support data rates of up to 2.4 Mbit/s [21] and can communicate in adverse environments [22]. The SUN-FSK-based Wi-SUN is referred to as the *existing Wi-SUN* in this study and the data-rate-enhanced Wi-SUN with the SUN-OFDM-based physical layer is referred to as the *next-generation Wi-SUN*.

The SUN-FSK-based existing Wi-SUN (widespread) and the SUN-OFDM-based next-generation Wi-SUN (expected to become widespread) are expected to coexist in the same frequency band in the same field [16], [23], as shown in Fig. 1. In this case, some nodes are required to handle different modulation schemes (that is, SUN-FSK and SUN-OFDM). A different modulation scheme coexistence scenario was envisioned in IEEE 802.15.4, which supports switching between SUN-FSK, SUN-OFDM, and offset quadrature phase-shift keying for SUN modes at a node (that is, mode switch mechanism) as an option [10]. A node that can support multiple modulation schemes is called a *heterogeneous node (Het-node)* in this study. Wi-SUN adopts carrier sense multiple access with collision avoidance (CSMA/CA) to avoid inter-node or inter-system interferences [10]. Suppose multiple nodes generate data simultaneously. In that case, CSMA/CA can avoid interference by employing a waiting time at each node. Consequently, some nodes experience large delays. However, this delay caused by CSMA/CA is undesirable for next-generation Wi-SUN, which requires highly responsive communication at high data rates. Therefore, a heterogeneous in-band full-duplex (Het-IBFD) system was proposed to simultaneously transmit and receive SUN-FSK and SUN-OFDM [23].

Numerous studies on IBFD are underway; however, most focused on IBFD between the same systems (that is, homogeneous IBFD) [24], [25], [26], [27], [28], [29], [30], [31], [32], [33], [34], [35]. For example, [25] proposed a balun-based self-interference (SI) cancellation scheme using a variable attenuator and delay line in an RF circuit and a digital SI cancellation scheme using an SI channel estimation technique to realize IBFD between IEEE 802.11b systems. Furthermore, [27] proposed an antenna domain SI cancellation scheme using a dual-polarized reflectarray to realize IBFD between LTE systems. Moreover, scheduling schemes to reduce SI and inter-cell interference to realize 5G-based IBFD have been applied to cellular systems [28], [29], [30]. However, [36] proposed SI cancellation schemes in the antenna and analog domains for the Het-IBFD system between IEEE 802.15.4 and IEEE 802.11 systems but not in the digital domain. We previously proposed a digital SI cancellation scheme for a Het-IBFD to transmit the next-generation Wi-SUN using IEEE 802.15.4-2020-compliant SUN-OFDM and simultaneously receive the existing Wi-SUN using IEEE 802.15.4g-compliant SUN-FSK [23]. To improve the high response performance of next-generation Wi-SUN, the reverse of [23] (a Het-IBFD system that can simultaneously transmit existing Wi-SUN and receive next-generation Wi-SUN) must be realized as well. However, to the best of our knowledge, such a system is yet to be investigated. The SI cancellation method proposed in [23] cannot be used because the transmitting and receiving systems are the reverse of the situation in [23].

This study proposes the Het-IBFD system to simultaneously transmit the existing Wi-SUN using IEEE 802.15.4g-compliant SUN-FSK and receive the next-generation Wi-SUN using IEEE 802.15.4-2020-compliant SUN-OFDM [25]. In particular, we propose a digital SI cancellation scheme based on high-precision SI channel estimation using the moving average method, which can be used when the SI signal is a SUN-FSK signal and the desired signal is a SUN-OFDM signal. Furthermore, we propose a highly efficient SUN-OFDM demodulation technique that considers the effects of residual SI. The proposed digital SI cancellation scheme is based on a successive interference cancellation (SIC) mechanism [25], [37], [38]. The SI signal received at the Het-node performing Het-IBFD is transmitted by its transmitter. Therefore, the transmission data in the SI signal contain known information, and a replica signal of the SI signal can be generated provided the SI channel can be estimated accurately. However, accurate SI channel estimation is challenging because the received signal contains both the SI (the SUN-FSK signal) and desired signals (the SUN-OFDM signal). Studies on auto-regressive moving average (ARMA) and neural network-based channel estimation methods as highly accurate channel estimation methods have been reported in [33] and [39]. However, these methods require a novel implementation of a special protocol for parameter adjustment (such as not receiving the desired signal during SI channel estimation [25]) and cannot be used to estimate and cancel the SI channel while receiving the desired signal, as assumed in this study.

The proposed SI channel estimation method is based on the feature that the time-domain waveform of SUN-OFDM has an amplitude characteristic close to the Gaussian property and the influence of this SUN-OFDM signal is reduced using the moving average method to achieve highly accurate SI channel estimation. In particular, the proposed SI channel estimation method using moving average is effective in Het-IBFD between SUN-FSK transmission and SUN-OFDM reception. The reasons for the novelty of this method are as follows:

- As earlier mentioned, only a few studies on Het-IBFD have been conducted.
- Even when considering homogeneous-IBFD between OFDM systems, our proposed method has not been reported because OFDM has a long symbol time, which renders sufficient averaging in the frequency domain challenging and thus does not lead to the same ideas as the proposed method.
- In the case of homogeneous-IBFD between FSK systems or Het-IBFD in which the desired signal is FSK and the SI signal is OFDM [22] because the FSK signal that interferes with the SI channel estimation has a constant amplitude and biased phase distribution, the moving average method is expected to be ineffective and no such method has been reported.

Furthermore, the SI channel is expected to fluctuate with time when surrounding structures and other objects move at high speeds. This may degrade the accuracy of SI channel estimation using the proposed method. Therefore, the second proposed highly efficient SUN-OFDM signal demodulation technique uses the spectral features of the SUN-FSK and SUN-OFDM signals to puncture subcarriers that are assumed to be contaminated by the SI signal when the SI signal is maintained.

The main contributions of this study are as follows:

- We propose a Het-IBFD system to simultaneously transmit the existing Wi-SUN using IEEE 802.15.4g-compliant SUN-FSK and receive the next-generation Wi-SUN using IEEE 802.15.4-2020-compliant SUN-OFDM.
- We propose an accurate SI channel estimation scheme using the moving averaging method and evaluate its performance using the packet error rate (PER) metric through Monte Carlo simulations.
- Finally, we propose a highly efficient SUN-OFDM demodulation technique that utilizes the spectrum characteristics of SUN-FSK and SUN-OFDM to reduce the effect of residual SI.

The remainder of this article is organized as follows. Section II provides an overview of the SUN-FSK and SUN-OFDM. Section III presents the assumed Het-IBFD system and designs the target values based on IEEE 802.15.4. Section IV proposes a SUN-OFDM receiver for the Het-IBFD including the proposed moving average-based SI signal cancellation and highly efficient SUN-OFDM demodulation schemes. Section V evaluates the Het-IBFD system with the proposed scheme and technique. Finally, the conclusions of the study are provided in Section VI.

II. OVERVIEW OF THE PHYSICAL LAYER OF EXISTING AND NEXT-GENERATION WI-SUN SYSTEMS

Here, we provide an overview of SUN-FSK (the physical layer compliant with IEEE 802.15.4g for the existing Wi-SUN) and SUN-OFDM (the most promising physical layer that is compliant with IEEE 802.15.4-2020 for next-generation Wi-SUN). Notably, the maximum transmit power for unlicensed radio is 20 mW (13 dBm) for existing and next-generation Wi-SUN in Japan [29]. The transmit power can be increased to 250 mW (24 dBm) with a particular low-power radio license. The transmit power is assumed as 20 mW for both Wi-SUN systems in this study.

TABLE 1. Main Parameters of IEEE 802.15.4g-Compliant SUN-FSK Operation Mode #2

Parameter	Values
Wireless transmission rate	100 kbit/s
Modulation	Filtered 2FSK
Modulation index	1.0
Channel spacing	400 kHz
Frequency band	920–928, 950–958 MHz

A. SUN-FSK (EXISTING WI-SUN PHYSICAL LAYER)

The IEEE 802.15.4g-compliant SUN-FSK, which has low-power consumption characteristics, is applied as the physical layer of the existing Wi-SUN. Approximately 22 million existing Wi-SUN terminals that utilize SUN-FSK have already been implemented in Tokyo. Channel equalization is not required in a slow-fading environment because SUN-FSK transmits information using multiple frequencies.

The main parameters of IEEE 802.15.4g-compliant SUN-FSK operating mode #2 are listed in Table 1 [10]. Operating mode #2 is specified by IEEE 802.15.4g and is the most widely used in Japan. In operating mode #2, the transmission data rate is 100 kbit/s and the channel spacing is 400 kHz. In Wi-SUN systems, a Gaussian filter is applied to strictly restrict the power leakage to adjacent channels. Forward error correction (FEC) is optionally used for low power consumption. Generally, FEC is not used for IEEE 802.15.4g-compliant SUN-FSK. In addition, we assume that the FEC is not applied to SUN-FSK.

B. SUN-OFDM (NEXT-GENERATION WI-SUN PHYSICAL LAYER)

The next-generation Wi-SUN is expected to support applications that require a higher data rate, real-time transmission, and high reliability in a mobile environment. Therefore, SUN-OFDM is a promising candidate. The maximum data rate was enhanced to 2.4 Mbit/s and standardized as IEEE 802.15.4-2020 in 2020 [21]. In general, SUN-OFDM consumes more transmission power than SUN-FSK. Therefore, next-generation Wi-SUN terminals are expected to have sufficient power supply [22].

The main parameters of IEEE 802.15.4-2020-compliant SUN-OFDM of option #3 are listed in Table 2, which is one of the four options [21]. The subcarrier spacing is constant at 31.25/3 kHz irrespective of the case, the base symbol (that is, one OFDM symbol without a cyclic prefix (CP)) length is 96 μs and the CP length is 24 μs (that is, 1/4 of the base symbol length). Because the channel spacing of option #3 is the same as that of the existing Wi-SUN operation mode #2, option #3 is the most promising. This study also assumed the

TABLE 2. Main Parameters of IEEE 802.15.4-2020-Compliant SUN-OFDM Option #3

Parameter	Values
Wireless transmission rate	200 kbit/s
Modulation and coding rate	QPSK, 1/2 (MCS3)
Normal bandwidth	281 kHz
Channel spacing	400 kHz
DFT size	32
Active tones	26
Pilot tones	2
Data tones	24
Base symbol length	96 μs
CP length	24 μs (1/4 of the base symbol length)
Frequency band	920–928 MHz

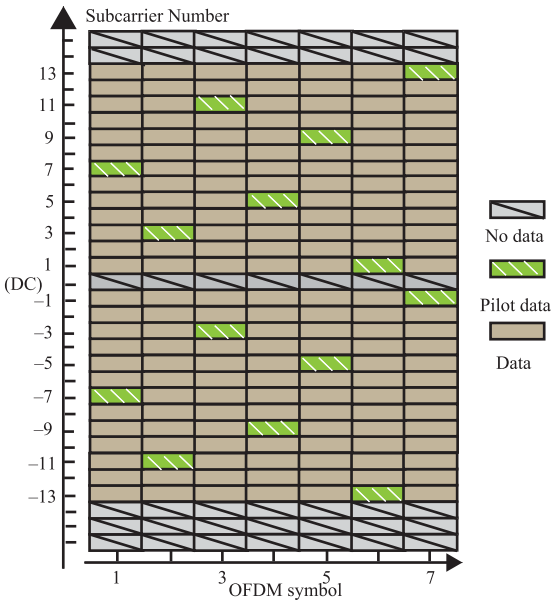

FIGURE 2. Pilot data allocation compliant with IEEE 802.15.4-2020 SUN-OFDM.

use of option #3. FEC (convolutional coding with a constraint length of 7) is mandatory for IEEE 802.15.4-2020-compliant SUN-OFDM. Pilot data allocation for option #3 is shown in Fig. 2. A scattered pilot method that dispersedly allocates pilot signals in the time and frequency domains is adopted. Seven symbols in the time domain form the basis of the pilot allocation and are repeated periodically. The channel is estimated using pilot signals and a long training field (LTF). Hence, the channels of data tones are estimated by interpolating or extrapolating in the time and frequency domains. Finally, the data tones are equalized using the estimated channels.

III. PROPOSED HETEROGENEOUS IBFD SYSTEM

A. HETEROGENEOUS IBFD FOR WI-SUN COEXISTENCE

As mentioned in Section I, the existing SUN-FSK-based Wi-SUN terminals and the next-generation SUN-OFDM-based Wi-SUN terminals will operate in the same frequency channel. These systems would be used according to the required data rate of each IoT device. As shown in Fig. 1, the data collection node (i.e., Het-node), which ultimately

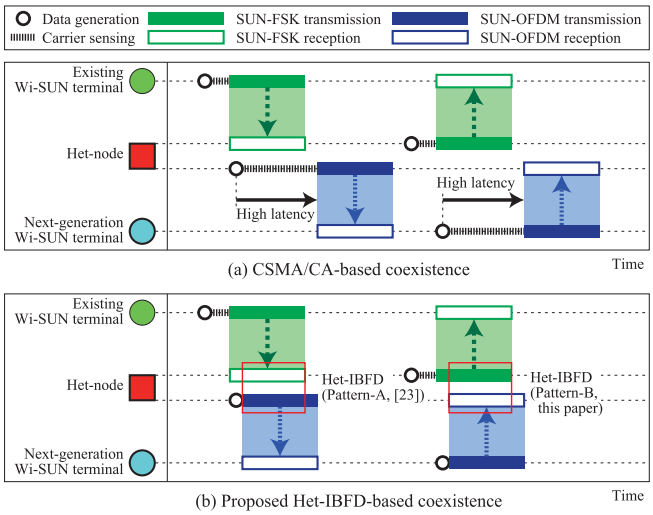

FIGURE 3. CSMA/CA-based coexistence and proposed Het-IBFD-based coexistence.

collects IoT data and connects to the Internet by means of a wide-area network (WAN) or other means, will need to communicate with both existing and next-generation Wi-SUN terminals. Currently, CSMA/CA is used to ensure the coexistence (i.e., interference avoidance) of these systems, as shown in Fig. 3(a). However, in the Het-node, if a request to receive or transmit SUN-OFDM occurs while SUN-FSK is being transmitted or received, it is necessary to wait for the completion of SUN-FSK transmission or reception, resulting in a large delay in SUN-OFDM communication.

Therefore, we have proposed a system that simultaneously transmits and receives SUN-OFDM and SUN-FSK in the Het-node using IBFD (i.e., Het-IBFD) when a request to transmit or receive SUN-OFDM occurs during the reception and transmission of SUN-FSK to reduce the latency of SUN-OFDM communication. As shown in Fig. 3(b), there are two types of Het-IBFD: Pattern-A (where SUN-FSK is received and SUN-OFDM is transmitted simultaneously) and Pattern-B (where SUN-FSK is transmitted and SUN-OFDM is received simultaneously). The former has already been proposed by the authors in [23]. In this article, we propose a signal processing to realize the latter Pattern-B and show its effectiveness through computer simulation evaluation.

B. PROPOSED SYSTEM CONFIGURATION

The proposed Het-IBFD system for Pattern-B is shown in Fig. 4. The Het-node, which manages two types of Wi-SUN systems, simultaneously performs SUN-OFDM reception and SUN-FSK transmission. This study proposes an SI canceller in the digital domain that suppresses the residual SI for the received signal after SI has been considerably suppressed by antenna and analog domain cancellations. For simplicity, quantization noise and noise figure were not considered in this study. Furthermore, the proposed system assumes that SI channel estimation for the SI canceller is performed during actual IBFD communication (We do not assume a proprietary

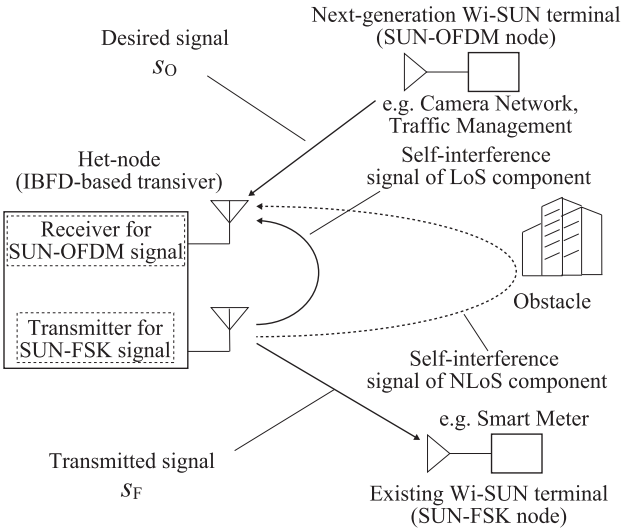

FIGURE 4. Proposed Het-IBFD system.

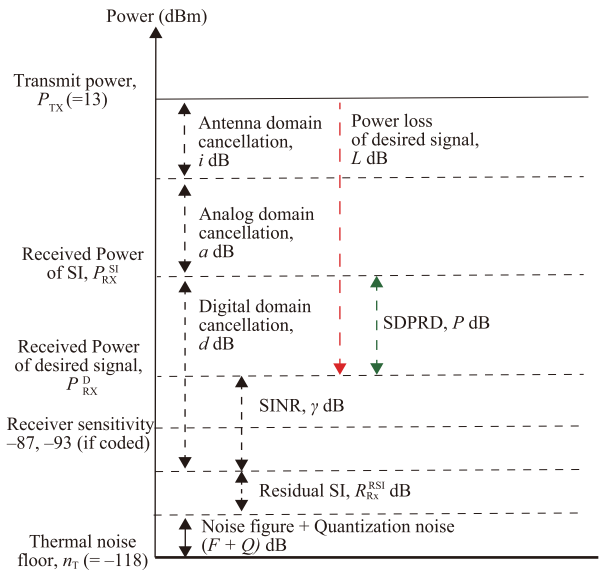

FIGURE 5. Level diagram of the proposed Het-IBFD.

protocol that performs SI channel estimation in half-duplex before full-duplex communication, as reported in [25], [33]).

The received signal at the Het-node $r[k]$ can be represented as follows:

$$r[k] = h_{SI}[k] * s_F[k] + h_D[k] * s_O[k] + n[k], \quad (1)$$

where k is the time sample index; $h_{SI}[k]$ and $s_F[k]$ represent the complex impulse response of the SI channel and SI signal (that is, the SUN-FSK signal of the existing-Wi-SUN), respectively; $h_D[k]$ and $s_O[k]$ represent complex impulse responses of the desired signal channel and desired signal (that is, the SUN-OFDM signal of the next-generation Wi-SUN), respectively. The additive white Gaussian noise (AWGN) is expressed as $n[k]$. $*$ denotes the convolution. Here, we focus on the SI channel $h_{SI}[k]$. As shown in Fig. 4, the SI channel comprises a line-of-sight (LoS) component (a direct wave) and non-LoS (NLoS) components (delayed waves). In general, the LoS component is stronger than the NLoS component provided the amount of antenna domain cancellation is small [35]. For example, suppose the propagation distance of the directed wave and the delayed wave are 1 m and 10 m, respectively. In that case, their time difference of arrival at the receiving antenna of the Het-node is approximately 0.03 μs because the propagation speed is approximately $c = 3.0 \times 10^8$ m/s. In contrast, the base symbol length of SUN-OFDM is 96 μs. Thus, even with a sufficiently high sampling rate of 10 Msample/s, the sampling interval is 0.1 μs, which is sufficiently larger than the time difference of arrival between the direct and delayed waves in the SI channel (0.03 μs). Therefore, (1) can be rewritten as follows:

$$r[k] = h_{SI}[k] s_F[k] + h_D[k] * s_O[k] + n[k]. \quad (2)$$

In the Het-IBFD system, the first term representing the SI component, $h_{SI}[k]s_F[k]$, must be removed to obtain the desired signal component, $h_D[k] * s_O[k]$.

The SI and desired signal power ratio in the digital domain (SDPRD), P (dB) is defined as follows:

$$P = P_{Rx}^{SI} - P_{Rx}^{D} = L - i - a, \quad (3)$$

$$P_{Rx}^{SI} = P_{Tx} - i - a, \quad (4)$$

$$P_{Rx}^{D} = P_{Tx} - L, \quad (5)$$

where P_{Rx}^{SI} (dBm) and P_{Rx}^{D} (dBm) are the received power of the SI and desired signals, respectively, P_{Tx} (dBm) is the transmission power ($P_{Tx} = 13$ dBm), L (dB) is the path loss of the desired signal, i (dB) is the SI cancellation level using antenna domain cancellation, and a (dB) is the SI cancellation level using analog domain cancellation. ARIB STD-T108 [40], which defines the requirements for the 920 MHz band utilization in Japan, specifies a carrier sense level of –80 dBm. Thus, the target received power of the desired signal P_{Rx}^{D}, is set to $-$ 80 dBm. Hence, the path loss of the desired signal can be calculated as $L = 93$ dB. Therefore, SDPRD can be calculated as $P = 40$ dB when the antenna and analog domain SI cancellations perform 53 dB suppression (that is, $i + a = 53$). In this study, we set $P = 30$, 40, and 50 dB for evaluation.

B. DESIGN OF THE TARGET SI SIGNAL CANCELLATION LEVEL

The level diagram of the proposed Het-IBFD is shown in Fig. 5. The residual SI signal must be canceled at the noise floor to demodulate the desired signal in the Het-IBFD. The thermal noise n_T (dBm) can be calculated as follows:

$$n_T = 10\log_{10}(KTB), \quad (6)$$

where K is Boltzmann's constant, T is the temperature, and B is the bandwidth. We set the channel spacing to 400 kHz. The thermal noise can be calculated as $n_T = -118$ dBm when the temperature is 288 K. Suppose the quantization noise and

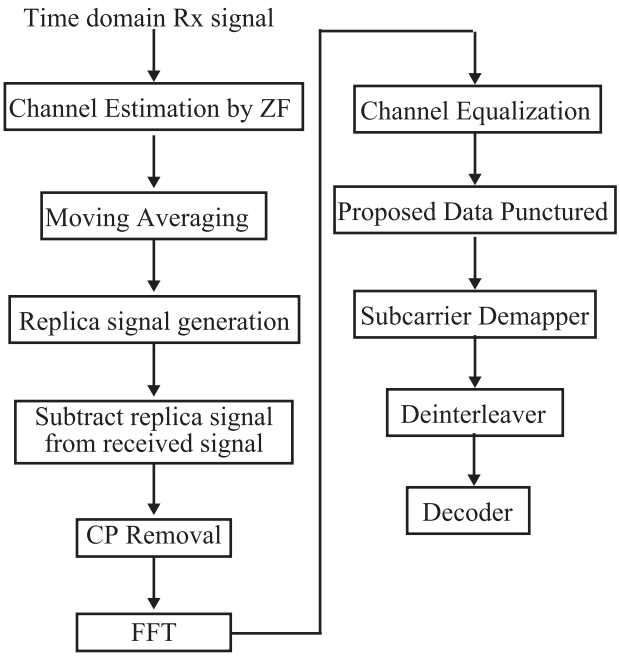

FIGURE 6. Block diagram of the receiver design.

noise figure are represented as Q (dB) and F (dB), respectively. In that case, the total noise floor n_{F} (dBm) can be expressed as follows:

$$n_{\mathrm{F}} = n_{\mathrm{T}} + Q + F. \tag{7}$$

Thus, the digital domain cancellation level d (dB) is calculated as follows:

$$d = P_{\mathrm{Rx}}^{\mathrm{SI}} - n_{\mathrm{F}} = P_{\mathrm{Tx}} - (n_{\mathrm{T}} + Q + F) - i - a - P_{\mathrm{Rx}}^{\mathrm{RSI}}, \tag{8}$$

where $P_{\mathrm{Rx}}^{\mathrm{RSI}}$ denotes the residual SI in the digital domain. Subsequently, the signal-to-noise plus interference power ratio (SINR) for the desired signal demodulation, γ (dB), can be calculated as follows:

$$\begin{aligned}\gamma &= P_{\mathrm{Rx}}^{\mathrm{D}} - n_{\mathrm{F}} - P_{\mathrm{Rx}}^{\mathrm{RSI}} \\ &= (P_{\mathrm{Tx}} - L) - (n_{\mathrm{T}} + Q + F) - P_{\mathrm{Rx}}^{\mathrm{RSI}} \\ &= P_{\mathrm{Tx}} - (P + i + a) - (n_{\mathrm{T}} + Q + F) - P_{\mathrm{Rx}}^{\mathrm{RSI}} \\ &= d - P. \end{aligned} \tag{9}$$

For simplicity, the quantization noise and noise figure were not considered in this study (that is, $Q = 0$ and $F = 0$).

IV. PROPOSED SUN-OFDM RECEIVER FOR THE HET-IBFD

This section proposes a SUN-OFDM receiver for Het-IBFD. A block diagram of the proposed SUN-OFDM receiver for the Het-IBFD is shown in Fig. 6. This receiver includes a proposed SIC-based SI cancellation scheme using the moving average technique and a proposed highly efficient SUN-OFDM demodulation scheme for Het-IBFD.

A. PROPOSED SI CANCELLATION SCHEME FOR HET-IBFD

1) BASIC PRINCIPLE

We propose a SIC signal separation technique-based digital SI cancellation using a novel SI channel estimation scheme for Het-IBFD. The SI channel $h_{\mathrm{SI}}[k]$ should be estimated to cancel the residual SI component, which is the first term of (2) represented by $h_{\mathrm{SI}}[k]s_{\mathrm{F}}[k]$. Suppose the SI channel can be estimated with high accuracy. In that case, a replica signal of the residual SI component can be generated because the transmitted signal s_{F} is a known signal at the receiver of the Het-node. Hence, the residual SI signal suppressed by SIC, $\hat{r}[k]$, can be represented as follows:

$$\hat{r}[k] = \left(h_{\mathrm{SI}}[k] - \widehat{h_{\mathrm{SI}}}[k]\right) s_{\mathrm{F}}[k] + h_{\mathrm{D}}[k] * s_{\mathrm{O}}[k] + n[k], \tag{10}$$

where $\widehat{h_{\mathrm{SI}}}[k]$ denotes the estimated SI channel. Suppose the estimation accuracy of $\widehat{h_{\mathrm{SI}}}[k]$ is high (that is $\widehat{h_{\mathrm{SI}}}[k] = h_{\mathrm{SI}}$). In that case, the first term of (10) is suppressed to zero. However, accurate SI channel estimation is generally challenging because the received signal contains both SI and the desired signal and AWGN. Generally, the SI channel is estimated as follows:

$$\widehat{h_{\mathrm{SI}}}[k] = \frac{r[k]}{s_{\mathrm{F}}[k]} = h_{\mathrm{SI}}[k] + p_{\mathrm{D}}[k], \tag{11}$$

$$p_{\mathrm{D}}[k] = \frac{h_{\mathrm{D}}[k] * s_{\mathrm{O}}[k] + n[k]}{s_{\mathrm{F}}[k]}, \tag{12}$$

where $p_{\mathrm{D}}[k]$ represents the SI channel estimation error to be reduced.

By averaging the estimated SI channel, $\widehat{h_{\mathrm{SI}}}[k]$ in the proposed scheme, the accuracy of the SI channel estimation is improved as follows:

$$\widehat{h_{\mathrm{SI}}}'[k] = \frac{1}{L_{\mathrm{M}}} \sum_{l=k-L_{\mathrm{M}}+1}^{k} \widehat{h_{\mathrm{SI}}}[l] = \overline{h_{\mathrm{SI}}}[k] + \overline{p_{\mathrm{D}}}[k], \tag{13}$$

$$\overline{h_{\mathrm{SI}}}[k] = \frac{1}{L_{\mathrm{M}}} \sum_{l=k-L_{\mathrm{M}}+1}^{k} h_{\mathrm{SI}}[l], \tag{14}$$

$$\overline{p_{\mathrm{D}}}[k] = \frac{1}{L_{\mathrm{M}}} \sum_{l=k-L_{\mathrm{M}}+1}^{k} p_{\mathrm{D}}[l], \tag{15}$$

where L_{M} is the moving average length. By setting L_{M} to a large value, $\overline{p_{\mathrm{D}}}[k]$ is close to zero because the statistical properties of $s_{\mathrm{O}}[k]$ (SUN-OFDM signal) and $n[k]$ (AWGN) amplitudes follow a Gaussian distribution. However, an excessively large L_{M} results in a significant processing delay at the receiver and a larger loss of information regarding the time fluctuation of the SI channel to be estimated. Therefore, L_{M} should be appropriately set for the environment.

2) ADAPTIVE MOVING AVERAGING LENGTH ESTIMATION

Here, we propose an appropriate moving average length estimation scheme for time-varying fading channels. The time fluctuation of the SI channel $\delta_{\mathrm{TF}}[k]$, in the time interval from

$k-1$ to k can be calculated as follows:

$$\delta_{\mathrm{TF}}[k] = h_{\mathrm{SI}}[k] - h_{\mathrm{SI}}[k-1]. \tag{16}$$

In the coherent time duration, the time fluctuation during the moving average length $\delta_{\mathrm{M}}[k]$, can be approximated as follows:

$$\delta_{\mathrm{M}}[k] = \sum_{l=k-L_{\mathrm{M}}+1}^{k} \delta_{\mathrm{TF}}[l] \cong L_M \overline{\delta_{\mathrm{TF}}}[k], \tag{17}$$

$$\overline{\delta_{\mathrm{TF}}}[k] = \frac{1}{N_{\mathrm{S}}} \sum_{l=k-N_{\mathrm{S}}+1}^{k} \delta_{\mathrm{TF}}[l], \tag{18}$$

where $\overline{\delta_{\mathrm{TF}}}[k]$ is the averaged $\delta_{\mathrm{TF}}[k]$ and N_{S} is the averaging length to calculate $\overline{\delta_{\mathrm{TF}}}[k]$. As shown in Section V-A, the SI channel is assumed to be obtained by the Rice channel and the Rice factor is assumed to be 20 dB. Moreover, the Doppler frequency is assumed to be less than 10 Hz. Hence, no abrupt channel time variations exist. Therefore, (17) and (18) are defined assuming the time interval is coherent and the channel fluctuates linearly. According to (17), when L_{M} is too long, the moving average results in a larger loss of information regarding the time fluctuation of the SI channel to be estimated. However, using the statistical characteristic of $p_{\mathrm{D}}[k]$, the residual SI channel estimation error owing to the desired signal after the moving averaging can be approximated as follows:

$$\overline{p_{\mathrm{D}}}[k] \cong \frac{1}{\sqrt{L_{\mathrm{M}}}} p_{\mathrm{D}}[k]. \tag{19}$$

According to (19), a large L_{M} can suppress the residual SI channel estimation error because of the desired signal. To set the optimal L_{M} while considering the balance between $\delta_{\mathrm{M}}[k]$ and $\overline{p_{\mathrm{D}}}[k]$, the following equation is obtained by solving the equilibrium equation with $\delta_{\mathrm{M}}[k] = \overline{p_{\mathrm{D}}}[k]$:

$$L_{\mathrm{M}}^{\mathrm{Opt}}[k] = \left(\frac{p_{\mathrm{D}}[k]}{\overline{\delta_{\mathrm{TF}}}[k]} \right)^{2/3}, \tag{20}$$

where $L_{\mathrm{M}}^{\mathrm{Opt}}[k]$ denotes the optimal L_{M}. Therefore, $p_{\mathrm{D}}[k]$ and $\overline{\delta_{\mathrm{TF}}}[k]$ should be estimated to obtain $L_{\mathrm{M}}^{\mathrm{Opt}}[k]$.

First, we provide the $p_{\mathrm{D}}[k]$ estimation method. This estimation is performed for every packet. Here, we define the time-sample index in the qth packet as k_q. The estimated SI channel for the first time sample of the qth packet, $\widehat{h_{\mathrm{SI}}}[k_q = 0]$, was used as the reference. The average of the absolute value of the difference between $\widehat{h_{\mathrm{SI}}}[0]$ and the estimated SI channel at each time sample is calculated as $p_{\mathrm{D}}[k_q]$:

$$\widehat{p_{\mathrm{D}}}[k_q] = \frac{1}{L_{\mathrm{P}}} \sum_{m=1}^{L_{\mathrm{P}}} \left| E_q(m) \right|, \tag{21}$$

$$E_q(k) = \widehat{h_{\mathrm{SI}}}[0] - \widehat{h_{\mathrm{SI}}}[k], \tag{22}$$

where $\widehat{p_{\mathrm{D}}}[k]$ is the estimated $p_{\mathrm{D}}[k]$, L_{P} is the average length of the $p_{\mathrm{D}}[k]$ estimation, and $E_q(k)$ is the error vector function with reference to $k_q = 0$. The effect of $\overline{\delta_{\mathrm{TF}}}[k]$ should be reduced when estimating $\widehat{p_{\mathrm{D}}}[k]$. As noted in (17), as $\overline{\delta_{\mathrm{TF}}}[k]$ increases with the time difference from the reference sample ($k_q = 0$), L_{P} should be considerably small. Notably, L_{P} is determined using a computer simulation in Section V.

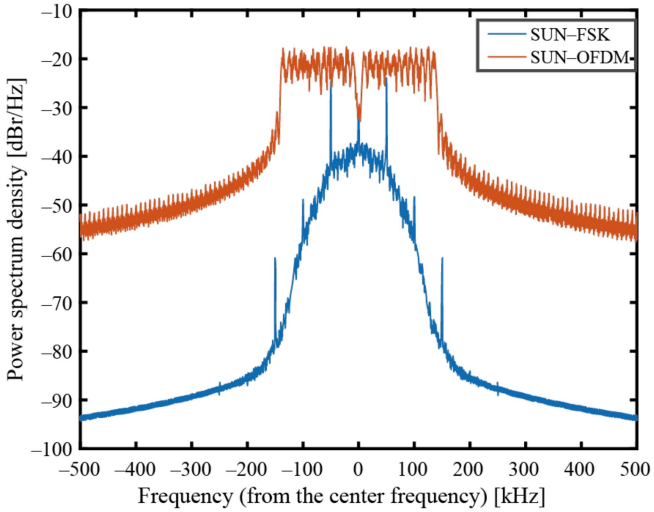

FIGURE 7. Spectrum of SUN-FSK and SUN-OFDM signals when $P = -20$ dB.

Second, we present a $\overline{\delta_{\mathrm{TF}}}[k]$ estimation method. This estimation is also performed for every packet. To accurately estimate $\overline{\delta_{\mathrm{TF}}}[k]$, we calculated the channel error vector as follows:

$$\widehat{\delta_{\mathrm{TF}}}[k_q] = \frac{1}{N_{\mathrm{S}}} \left| - \sum_{m=N_{\mathrm{S}}-L_{\mathrm{T}}+1}^{N_{\mathrm{S}}} E_q(m) \right|, \tag{23}$$

where L_{T} is the average length for time-fluctuation estimation during the moving average and $\widehat{\delta_{\mathrm{TF}}}[k_q]$ is the estimated $\overline{\delta_{\mathrm{TF}}}[k]$. L_{T} is determined through a computer simulation in Section V. After estimating $\widehat{p_{\mathrm{D}}}[k_q]$ and $\widehat{\delta_{\mathrm{TF}}}[k]$, the estimated moving averaging length, $\widehat{L_{\mathrm{M}}^{\mathrm{Opt}}}[k]$, can be obtained using (20).

B. THE PROPOSED HIGHLY EFFICIENT SUN-OFDM DEMODULATION SCHEME FOR HET-IBFD

An appropriate $\widehat{L_{\mathrm{M}}^{\mathrm{Opt}}}[k]$ performs accurate SI cancellation and the demodulation quality of the desired signal can be improved. However, suppose the time variation of the SI channel is faster than expected (the Doppler frequency of the channel is large) or the packet length is too short to ensure a sufficient moving average length. In that case, the SI component is maintained. Therefore, we propose a method to demodulate the desired signal with high quality when some SI is maintained using the SUN-OFDM and SUN-FSK spectral features.

The spectrum of SUN-OFDM and SUN-FSK when $P = -20$ dB, assuming that all SI cancellation schemes are applied in each domain is shown in Fig. 7. Here, the SI signal (that is, SUN-FSK) power can be suppressed to a level of 20 dB lower than the desired signal (SUN-OFDM) power. However, because the SUN-FSK signal contains a large line spectrum

(particularly at ±50 kHz from the center frequency), the demodulation quality of some subcarriers of the desired signal may be significantly degraded. A subcarrier number of ±5 is largely contaminated by the SUN-FSK signal because the subcarrier spacing of SUN-OFDM is 31.25/3 kHz, that is, the SINR of a subcarrier number of ±5 is considerably smaller than other SINR per subcarrier. Thus, in the proposed scheme, the SUN-OFDM signals at a subcarrier number of ±5 are punctured. Punctured data can be demodulated at the receiver because FEC is mandatory for SUN-OFDM. We refer to the proposed highly efficient SUN-OFDM demodulation scheme as the *data puncturing (DP) scheme* hereinafter.

V. PERFORMANCE EVALUATION THROUGH COMPUTER SIMULATIONS

The performance of the proposed Het-IBFD system was evaluated through computer simulations. The channel model and estimation method for the desired signal was examined before evaluation. Next, the effectiveness of the proposed method was demonstrated by showing the PER when the appropriate moving average length was used after demonstrating the existence of different optimal moving average lengths for several Doppler frequency conditions. In addition, we evaluated the proposed method to determine the moving average length to be applied under arbitrary Doppler frequency conditions.

A. CHANNEL MODELS FOR HET-IBFD

1) SI CHANNEL

As shown in Fig. 4, the SI channel comprises LoS and NLoS components. Such channels can be modeled using Rice fading, and the Rice factor (the power ratio of the LoS and NLoS components) in indoor environments was reported to be 20–25 dB [27]. The Rice factor was assumed to be 20 dB in this study.

Suppose moving objects exist around the Het-node. In that case, a Doppler shift f_{D} (Hz) occurs as follows:

$$f_{\mathrm{D}} = \frac{c}{f_{\mathrm{c}}} v, \tag{24}$$

where $c = 3.0 \times 10^8$ m/s is the propagation speed (speed of light), $f_{\mathrm{c}} = 920$ MHz is the center frequency, and v m/s is the velocity of moving objects. The following three environments were assumed in this study:

1) An environment with almost no moving object, $f_{\mathrm{D}}^{\mathrm{SI}} = 0.34$ Hz ($v = 0.4$ km/h).
2) An environment with moving objects, such as pedestrians, $f_{\mathrm{D}}^{\mathrm{SI}} = 3.4$ Hz ($v = 4$ km/h).
3) An environment with moving objects, such as bicycles in addition to pedestrians, $f_{\mathrm{D}}^{\mathrm{SI}} = 6.8$ Hz ($v = 8$ km/h), where $f_{\mathrm{D}}^{\mathrm{SI}}$ is the Doppler frequency of the SI channel.

2) DESIRED SIGNAL CHANNEL

For the desired signal channel, we consider a GSM typical urban (TU) environment shown in Table 3 [15]. The Doppler frequencies of the desired signal channel, $f_{\mathrm{D}}^{\mathrm{DS}}$, are 3.4 Hz and 6.8 Hz, assuming the moving objects are pedestrians and bicycles, respectively. The combinations of Doppler frequencies for the SI and desired signal channels in this evaluation are listed in Table 4.

TABLE 3. GSM TU Channel Model

Parameter	Path1	Path2	Path3	Path4	Path5	Path6
Delay Time (μs)	0	0.2	0.5	1.6	2.3	5.0
Relative Power (dB)	–3	0	–2	–6	–8	–10

TABLE 4. Combinations of Doppler Frequencies for Evaluation

	Desired signal channel	SI channel
Case 1	$f_{\mathrm{D}}^{\mathrm{DS}} = 3.4$ Hz	$f_{\mathrm{D}}^{\mathrm{SI}} = 0.34$ Hz
Case 2	$f_{\mathrm{D}}^{\mathrm{DS}} = 3.4$ Hz	$f_{\mathrm{D}}^{\mathrm{SI}} = 3.4$ Hz
Case 3	$f_{\mathrm{D}}^{\mathrm{DS}} = 6.8$ Hz	$f_{\mathrm{D}}^{\mathrm{SI}} = 6.8$ Hz

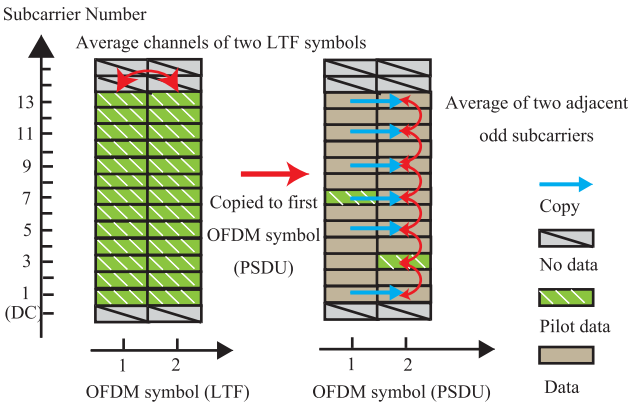

FIGURE 8. Channel estimation procedure for the desired signal channel.

B. CHANNEL ESTIMATION METHOD FOR THE DESIRED SIGNAL

The communication quality of the desired signal (that is, SUN-OFDM) after SI cancellation was evaluated using the PER to evaluate the performance of the proposed SI cancellation scheme. Therefore, channel estimation and equalization of the desired signal should be performed. In this evaluation, the channel estimation and equalization based on [20] were performed in the frequency domain.

The channel estimation procedure estimation for the desired signal channel is shown in Fig. 8. First, the channel of each subcarrier is estimated using an LTF with two OFDM symbols. Subsequently, the estimated channels for the two OFDM symbols are averaged to reduce the effect of noise. This is used as the estimated channel for the first OFDM symbol portion of the PSDU, as follows:

$$\widehat{H_{\mathrm{D}}}(l, 0) = \frac{1}{2}\left(\widehat{H_{\mathrm{D}}}(l, -2) + \widehat{H_{\mathrm{D}}}(l, -1)\right), \tag{25}$$

where $\widehat{H_{\mathrm{D}}}(l, m)$ is the estimated desired signal channel in the frequency domain of the lth subcarrier of the mth OFDM symbol, $m = -2$, $m = -1$, and $m = 0$ indicate the first LTF

TABLE 5. Parameters to Obtain an Appropriate Moving Average Length

Parameter	Values
Doppler frequency of the SI signal, $f_{\mathrm{D}}^{\mathrm{SI}}$	0.34 Hz (Case 1), 3.4 Hz (Case 2), 6.8 Hz (Case 3)
Doppler frequency of the desired signal	3.4 Hz
Rice factor	20 dB
PSDU size	250 octets

symbol, second LTF symbol, and first OFDM symbol of PSDU, respectively.

Second, the estimated channel in the odd-numbered subcarrier of the mth OFDM symbol is copied and used as the estimated channel in the same subcarrier of the $(m+1)$th OFDM symbol as follows:

$$\widehat{H_{\mathrm{D}}}(l, m+1) = \widehat{H_{\mathrm{D}}}(l, m), \quad l \in \{-13, -11, -9, \ldots 9, 11, 13\}. \tag{26}$$

The channel estimated using the pilot subcarrier is used without copying in the case in which a pilot symbol exists in the subcarrier to be copied.

Finally, the channels for even-numbered subcarriers of the $(m+1)$th OFDM symbol are obtained by averaging the estimated channels of the adjacent subcarriers, as follows:

$$\widehat{H_{\mathrm{D}}}(l, m+1) = \frac{1}{2}\left(\widehat{H_{\mathrm{D}}}(l+1, m+1) + \widehat{H_{\mathrm{D}}}(l-1, m+1)\right), \quad l \in \{-12, -10, -8, \ldots 8, 10, 12\}. \tag{27}$$

C. PER PERFORMANCE EVALUATION WITH APPROPRIATE MOVING AVERAGE LENGTH

First, we evaluated the PER performance of the desired signal in the Het-IBFD using the proposed SI cancellation scheme. An appropriate moving average length was obtained through computer simulations. The simulation parameters are listed in Tables 1, 2 and 5. The number of iterations in each simulation is 50000.

1) APPROPRIATE MOVING AVERAGE LENGTH

The PER of the desired signal as a function of the moving average length for each Doppler frequency when $P = 40$ dB is shown in Fig. 9. In this evaluation, the DP scheme was not applied, and E_{b}/N_0 for the desired signal was set to 100 dB. As mentioned in Section IV-A-1, the moving average length is a trade-off between $\overline{p_{\mathrm{D}}}[k]$ and $\overline{\delta_{\mathrm{TF}}}[k]$ reductions. Therefore, the PER characteristics shown in Fig. 9 are downward convex functions. As the Doppler frequency increased, the optimal moving average length $L_{\mathrm{M}}^{\mathrm{Opt}}[k]$ decreased because of larger channel time fluctuations $\overline{\delta_{\mathrm{TF}}}[k]$. When $f_{\mathrm{D}}^{\mathrm{SI}} = 6.8$, 3.4, and 0.34 Hz, the appropriate moving average lengths were 35, 40, and 100 (the maximum value within the set values), respectively. The appropriate moving average lengths for $P = 30$, 40, and 50 dB with the Doppler frequencies of 0.34, 3.4, and 6.8 Hz are summarized in Table 6, respectively.

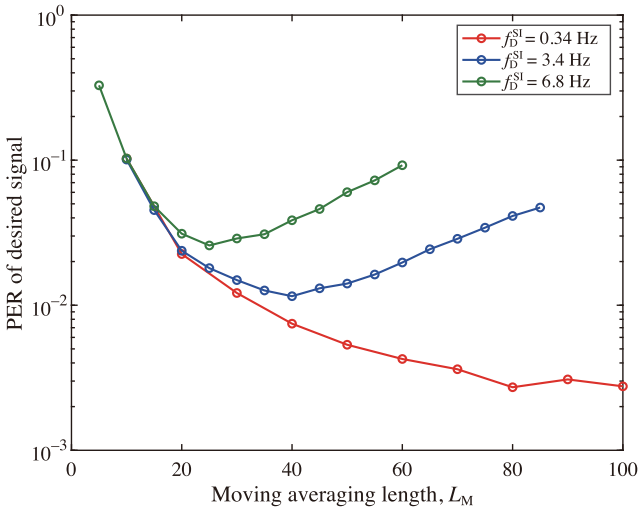

FIGURE 9. PER of the desired signal as a function of the moving average length for each Doppler frequency when $P = 40$ dB.

TABLE 6. Appropriate Moving Average Lengths

SDPRD, P (dB)	Doppler frequency of the SI channel, $f_{\mathrm{D}}^{\mathrm{SI}}$ (Hz)	Appropriate moving average length, $L_{\mathrm{M}}^{\mathrm{Opt}}[k]$
30	0.34 (Case 1)	100
30	3.4 (Case 2)	60
30	6.8 (Case 3)	50
40	0.34 (Case 1)	100
40	3.4 (Case 2)	40
40	6.8 (Case 3)	35
50	0.34 (Case 1)	100
50	3.4 (Case 2)	25
50	6.8 (Case 3)	20

TABLE 7. Minimum E_{b}/N_0 to Achieve PER <10%

Doppler Frequency	w/o MA and DP	w/ MA, w/o DP	w/ MA and DP
Case 1	NaN	16.8 dB	17.4 dB
Case 2	NaN	17.9 dB	18.3 dB
Case 3	NaN	19.5 dB	19.5 dB

2) PER PERFORMANCE

The PER of the desired signal as a function of E_{b}/N_0 for each Doppler frequency when $P = 40$ dB is shown in Fig. 10. The appropriate moving average length, shown in Table 6, was applied.

The required PER was 10% as defined by Wi-SUN specification. The minimum E_{b}/N_0 for the desired signal to achieve PER $< 10\%$ is listed in Table 7. When the conventional SIC was applied without the proposed schemes, PER $< 10\%$ could not be achieved in any Doppler frequency case. PER $< 10\%$ could be achieved in any Doppler frequency case by introducing the proposed moving average-based SI cancellation scheme (referred to as the *MA scheme* hereinafter).

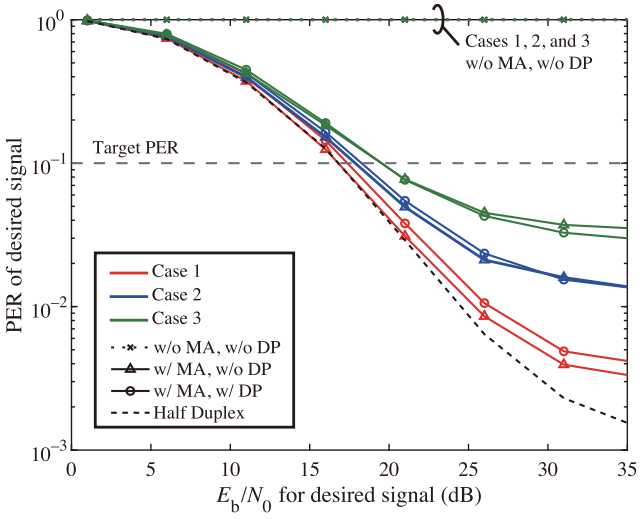

FIGURE 10. PER of the desired signal as a function of E_b/N_0 for the desired signal of each Doppler frequency case when $P = 40$ dB.

TABLE 8. Actual Values of $p_D[k_q]$ and $\delta_{TF}[k_q]$

Doppler frequency of the SI signal, f_D^{SI} (Hz)	$p_D[k_q]$	$\delta_{TF}[k_q]$
0.34	0.0063	0.00026
3.4	0.0063	0.0027
6.8	0.0063	0.0054
34	0.0063	0.0268

D. PER PERFORMANCE EVALUATION WITH THE ESTIMATED MOVING AVERAGE LENGTH

Here, we searched for adequate variables of L_P and L_T to adaptively estimate the moving averaging length and comprehensively evaluated the PER performance with the estimated moving average length.

1) ADEQUATE L_P AND L_T

The simulation parameters for this evaluation are listed in Table 5. Furthermore, we performed an evaluation under a Doppler frequency of 34 Hz. The actual values of $p_D[k_q]$ and $\delta_{TF}[k_q]$ when N_S was set to 200 are listed in Table 8 for each Doppler frequency. The SI channel estimation error, $p_D[k_q] - \widehat{p_D}[k_q]$, as a function of the averaging length, L_P and the estimation error of the time fluctuation of the SI channel, $\delta_{TF}[k_q] - \widehat{\delta_{TF}}[k_q]$, as a function of the average length, L_T, are shown in Fig. 11(a) and (b), respectively. The value of each estimation error for each Doppler frequency converges approximately at an average length of 10, as shown in Fig. 11(a) and (b). Therefore, $L_P = L_T = 10$.

2) PER PERFORMANCE

The simulation parameters are listed in Table 5. The SDPRD was set to $P = 30$, 40, and 50 dB, and N_S was set to 200. The PER of the desired signal as a function of E_b/N_0 for $P = 30$, 40, and 50 dB, are shown in Figs. 12–14 respectively. For comparison, the results obtained using the appropriate moving

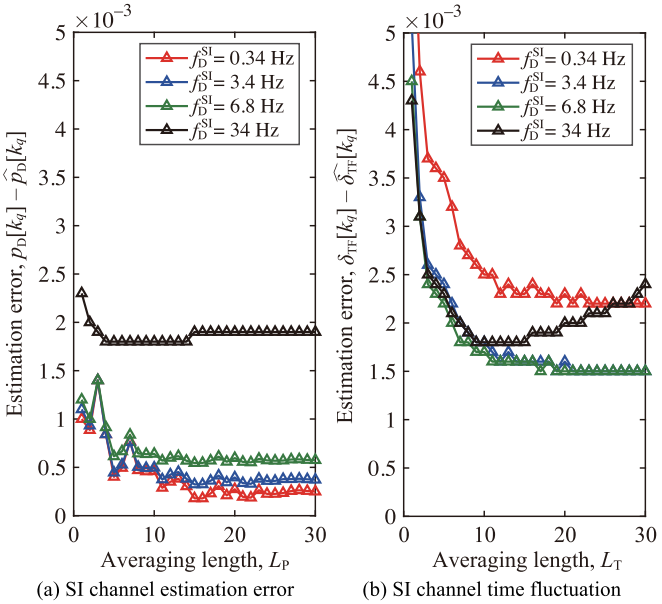

FIGURE 11. Estimation Errors as a function of the average length.

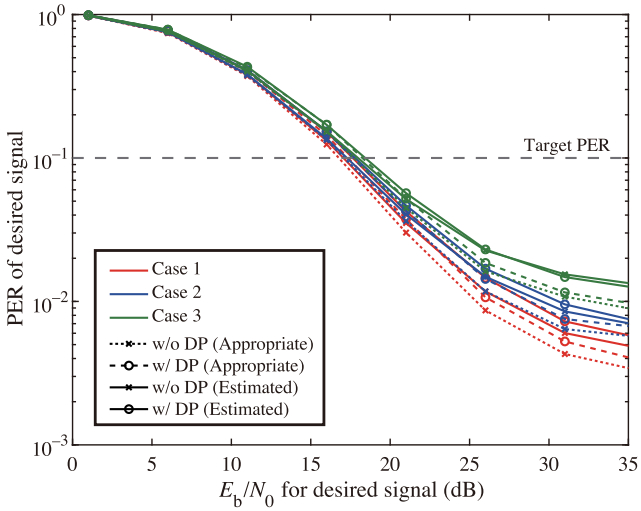

FIGURE 12. PER of the desired signal as a function of E_b/N_0 when $P = 30$ dB.

average length shown in Table 6 and the estimated moving average length with $L_P = L_T = 10$ are shown in Figs. 12–14.

First, in all the cases ($P = 30$, 40, and 50 dB), the PER with the estimated moving average length, with or without the adaptation of the DP method, asymptotically approached the PER with the appropriate moving average length. Therefore, the proposed adaptive moving average length estimation method is appropriate.

Next, we examined the effectiveness of the DP method. As shown in Figs. 12–14, the DP method can improve the PER in Case 3 when $P = 30$ and 40 dB and in Cases 2 and 3 when $P = 50$ dB. Particularly, in Case 3 when $P = 50$ dB, the target PER of 10% can be achieved only by applying the proposed DP method with the appropriate moving average length. Furthermore, with the estimated moving average length, the

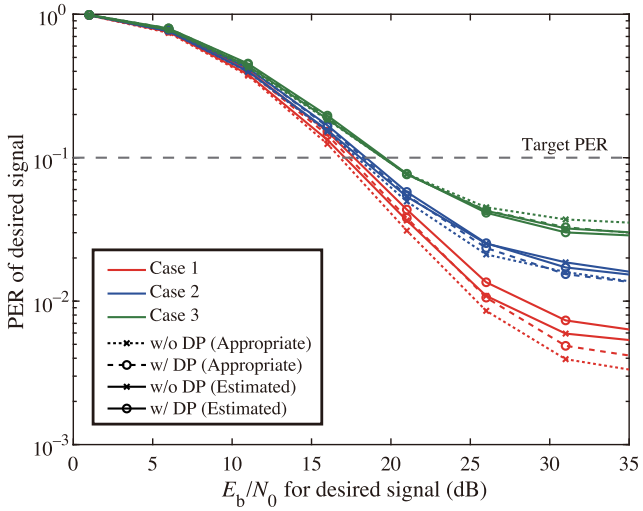

FIGURE 13. PER of the desired signal as a function of E_b/N_0 when P = 40 dB.

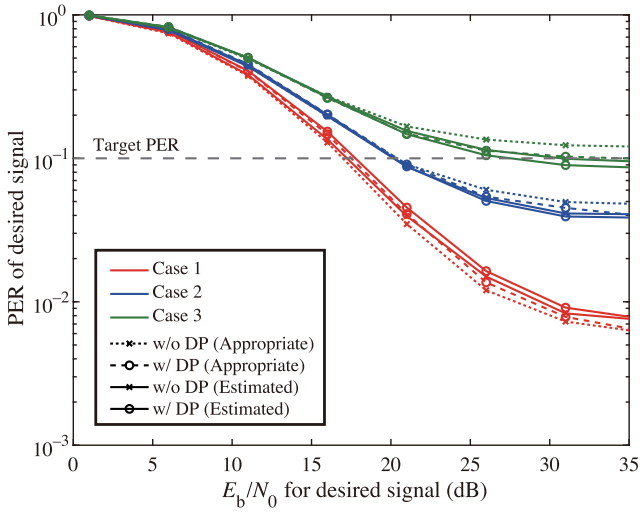

FIGURE 14. PER of the desired signal as a function of E_b/N_0 when P = 50 dB.

proposed DP method improves E_b/N_0 to achieve the target PER of 10% by over 5 dB. Conversely, in the other cases, PER exhibited better characteristics when the DP method was not used. This is because the DP method is effective when the residual SI is large. From (20) and Table 6, the SDPRD increases ($p_D[k_q]$ decreased) or Doppler frequency increased ($\overline{\delta_{TF}}[k]$ increased) when the adequate moving averaging length decreased. Small moving averaging results in large SI signal residuals. When the residual SI was large, the PER could be improved using the DP method to eliminate the influence of a particularly large line spectrum of the SUN-FSK signal, which is the SI. However, when the residual SI was small, the PER deteriorated owing to the unnecessary puncturing of OFDM subcarriers.

Finally, we discussed the amount of SI cancellation required in the antenna and analog domains when using the proposed method. For example, when P = 50 dB and considering the Doppler frequency of Case 1, the proposed schemes could achieve an SINR of 17 dB, resulting in PER of 10%, as shown in Fig. 14. Therefore, referring to (9), the proposed digital SI canceller could achieve 17 + 50 = 67 dB of SI cancellation. Therefore, the antenna and analog domain SI cancellation required a reduction in the SI of at least 13 – (–118 + 67) = 64 dB, referring to (4), when P_{Tx} = 13 dBm and n_T = –118 dBm. This is realistic considering existing studies and development cases of SI cancellers in the antenna analog domain.

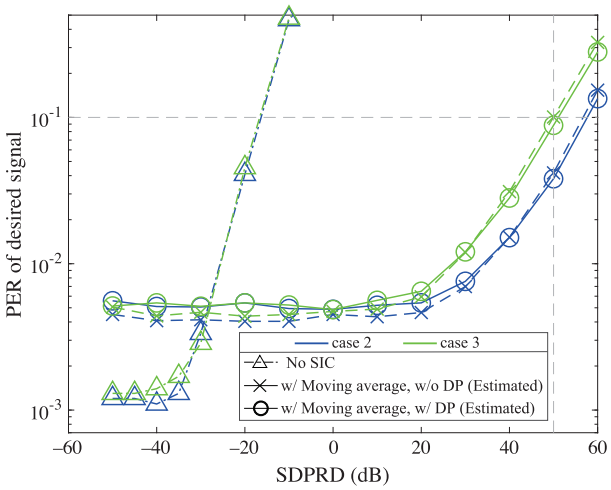

FIGURE 15. PER of the desired signal as a function of SDPRD.

E. PER PERFORMANCE EVALUATION FOR SDPRD

Here, we evaluated the acceptable SDPRD with the proposed SI canceller. Further, we discussed the requirement of an antenna and analog domain cancellation. The parameters are the same as in Section V-D-2. At least 64 dB of total SI cancellation was required in the antenna and analog domains in Section V-D-2. Hence, from (3), SDPRD is (L – 64) dB. Assuming next-generation Wi-SUN terminals will be used at more than 1 m from the Het-node, the path loss is highly unlikely to be less than 30 dB. Therefore, an SDPRD of at least (30 – 64 =) –34 dB should be assumed. Here, we considered the margin and evaluated the SDPRD above –50 dB.

The PER with and without the proposed SI canceller as a function of SDPRD for cases 2 and 3 is shown in Fig. 15. In the case of SDPRD smaller than –30 dB, the PER was better when the proposed SI canceller was not applied than when it was applied. However, the proposed SI cancellation could satisfy the target PER of less than 0.1 even when the SI signal power was smaller than the desired signal (SDPRD is less than 0 dB). Notably, when SDPRD was very small, the proposed method could estimate the SI channel while suppressing the desired signal by moving averaging. Therefore, the estimation of the SI channel could be somewhat accurate even when the SI signal level is less than the desired signal level.

VI. CONCLUSION

This study proposed the Het-IBFD system to simultaneously transmit the existing Wi-SUN using IEEE 802.15.4g-compliant SUN-FSK and receive the next-generation Wi-SUN using IEEE 802.15.4-2020-compliant SUN-OFDM. We proposed a digital SI cancellation scheme based on high-precision SI channel estimation using the moving average method, which could be used when the SI signal was an SUN-FSK signal and the desired signal was an SUN-OFDM signal. Furthermore, we proposed a highly efficient SUN-OFDM demodulation technique that considered the effects of the residual SI. The proposed methods were evaluated through computer simulations and the proposed schemes achieved an SI cancellation of 67 dB in the digital domain when $P = 50$ dB. Based on the results of this study, the existing Wi-SUN and next-generation Wi-SUN could coexist efficiently, which is expected to improve the throughput and responsiveness of next-generation Wi-SUN systems employing SUN-OFDM.

REFERENCES

[1] S. Kumar, P. Tiwari, and M. Zymbler, "Internet of things is a revolutionary approach for future technology enhancement: A review," *J. Big Data*, vol. 6, Dec. 2019, Art. no. 111.

[2] Cisco, "Cisco annual internet report (2018–2023)," Mar. 2020. Accessed: Jun. 13, 2023. [Online]. Available: https://www.cisco.com/c/en/us/solutions/collateral/executive-perspectives/annual-internet-report/white-paper-c11-741490.html

[3] Wi-Fi Alliance. Accessed: Jun. 13, 2023. [Online]. Available: https://www.wi-fi.org/

[4] *Connectivity Standards Alliance (CSA-IoT)*. Accessed: Jun. 13, 2023. [Online]. Available: https://csa-iot.org/

[5] LoRa Alliance. Accessed: Jun. 13, 2023. [Online]. Available: https://lora-alliance.org/about-lorawan/

[6] Sigfox. Accessed: Jun. 13, 2023. [Online]. Available: https://www.sigfox.com/en

[7] Wi-SUN Alliance. Accessed: Jun. 13, 2023. [Online]. Available: https://wi-sun.org/

[8] A. R. Biswas and R. Giaffreda, "IoT and cloud convergence: Opportunities and challenges," in *Proc. IEEE World Forum Internet Things*, 2014, pp. 375–376.

[9] *IEEE Computer Society*, IEEE Standard 802.11™-2020, Dec. 2020.

[10] *IEEE Computer Society*, IEEE Standard 802.15.4™-2015, Dec. 2015.

[11] S. Lee, B. Kim, M. K. Oh, Y. Jeon, and S. Choi, "Implementation of IEEE 802.15.4g wireless communication platform for smart utility service," in *Proc. IEEE 3rd Int. Conf. Consum. Electron.*, 2013, pp. 287–289.

[12] R. Bikmetov, M. Y. A. Raja, K. Kazi, B. Chowdhury, and J. Enslin, "Dynamic prediction capabilities of smart metering infrastructure," in *Proc. IEEE North Amer. Power Symp.*, 2015, pp. 1–5.

[13] H. Harada et al., "IEEE 802.15.4g based Wi-SUN communication systems," *IEICE Trans. Commun.*, vol. E100-B, no. 7, pp. 1032–1043, Jul. 2017.

[14] R. Okumura, K. Mizutani, and H. Harada, "feasibility study of Wi-SUN JUTA profile-compliant F-RIT protocol," *IEICE Trans. Commun.*, vol. E104-B, no. 10, pp. 1354–1365, Oct. 2021.

[15] K. Mochizuki, K. Obata, K. Mizutani, and H. Harada, "Development and field experiment of wide area Wi-SUN system based on IEEE 802.15.4g," in *Proc. IEEE 3rd World Forum Internet Things*, 2016, pp. 76–81.

[16] H. Ochiai, K. Mizutani, and H. Harada, "Wi-SUN FAN multi-hop network in coexistence of IEEE 802.15.4 FSK and OFDM transmission schemes," in *Proc. IEEE 24th Int. Symp. Wireless Pers. Multimedia Commun.*, 2021, pp. 1–6.

[17] T. Junjalearnvong, R. Okumura, K. Mizutani, and H. Harada, "Performance evaluation of multi-hop network configuration for Wi-SUN FAN systems," in *Proc. IEEE 16th Annu. Consum. Commun. Netw. Conf.*, 2019, pp. 1–6.

[18] H. Ochiai, K. Mizutani, R. Okumura, K. Mizutani, and H. Harada, "A high-speed Wi-SUN FAN network by highly-dense frequency hopping," in *Proc. IEEE 92nd Veh. Technol. Conf.*, 2020, pp. 1–5.

[19] Y. Xiang, R. Okumura, K. Mizutani, and H. Harada, "Data rate enhancement of FSK transmission scheme for IEEE 802.15.4-based field area network," *IEEE Sens. J.*, vol. 21, no. 7, pp. 9600–9611, Apr. 2021.

[20] S. Kadoi, H. Ochiai, R. Okumura, K. Mizutani, and H. Harada, "IEEE 802.15.4g/4x-based orthogonal frequency-division multiplexing transmission scheme for wide-area and mobile IoT communication systems," *IEEE Internet Things J.*, vol. 9, no. 14, pp. 12673–12683, Jul. 2022.

[21] *IEEE Computer Society*, IEEE Standard 802.15.4 ™ -2020, Jul. 2020.

[22] J. Muñoz, T. Chang, X. Vilajosana, and T. Watteyne, "Evaluation of IEEE802.15.4g for environmental observations," *Sensors*, vol. 18, no. 10, pp. 3468, Oct. 2018.

[23] Y. Morikawa, K. Mizutani, and H. Harada, "Highly efficient demodulation scheme for in-band full-duplex using heterogeneous wireless communication schemes," in *Proc. IEEE 94th Veh. Technol. Conf.*, 2021, pp. 1–5.

[24] D. Bharadia, E. McMilin, and S. Katti, "Full duplex radios," in *Proc. ACM SIGCOMM Conf.*, 2013, pp. 375–386.

[25] M. Jain et al., "Practical, real-time, full duplex wireless," in *Proc. 17th Annu. Int. Conf. Mobile Comput. Netw.*, 2011, pp. 301–312.

[26] A. Sabharwal, P. Schniter, D. Guo, D. W. Bliss, S. Rangarajan, and R. Wichman, "In-band full-duplex wireless: Challenges and opportunities," *IEEE J. Sel. Areas Commun.*, vol. 32, no. 9, pp. 1637–1652, Sep. 2014.

[27] N. Zarifeh, M. Alissa, M. Khaliel, and T. Kaiser, "Self-interference mitigation in full-duplex base-station using dual polarized reflectarray," in *Proc. IEEE 11th German Microw. Conf.*, 2018, pp. 180–183.

[28] T. Matsumura, H. Kuriki, K. Mizutani, and H. H, "Macro-cell capacity enhancement with dynamic full-duplex cellular system," in *Proc. IEEE 21st Int. Symp. Wireless Pers. Multimedia Commun.*, 2018, pp. 336–341.

[29] K. E. Kolodziej, A. U. Cookson, and B. T. Rerry, "Machine learning for accelerated IBFD tuning in 5G flexible duplex networks," in *Proc. IEEE/MTT-S Int. Microw. Symp.*, 2020, pp. 691–694.

[30] Y. Arakawa, K. Nishikori, K. Mizutani, T. Matsumura, and H. Harada, "An initial study of dynamic-duplex cellular system on 5G NR downlink in high SHF band," in *Proc. IEEE 18th Annu. Consum. Commun. Netw. Conf.*, 2021, pp. 1–2.

[31] K. Mizutani and H. Harada, "Quantization noise reduction by digital signal processing-assisted analog-to-digital converter for in-band full-duplex wireless communications," *IEEE Trans. Wireless Commun.*, vol. 21, no. 8, pp. 6643–6655, Aug. 2022.

[32] Z. Zhang, K. Long, A. Vasilakos, and L. Hanzo, "Full-duplex wireless communications: Challenges, solutions, and future research directions," *Proc. IEEE*, vol. 104, no. 7, pp. 1369–1409, Jul. 2016.

[33] V. Tapio and M. Juntti, "Non-linear self-interference cancelation for full-duplex transceivers based on Hammerstein-Wiener model," *IEEE Commun. Lett.*, vol. 25, no. 11, pp. 3684–3688, Nov. 2021.

[34] K. E. Kolodziej, B. T. Perry, and J. S. Herd, "In-band full-duplex technology: Techniques and systems survey," *IEEE Trans. Microw. Theory Techn.*, vol. 67, no. 7, pp. 3025–3041, Jul. 2019.

[35] E. Everett, A. Sahai, and A. Sabharwal, "Passive self-interference suppression for full-duplex infrastructure nodes," *IEEE Trans. Wireless Commun.*, vol. 13, no. 2, pp. 680–694, Feb. 2014.

[36] J. Kim W. Jeon, K. J. Park, and J. P. Choi, "Coexistence of full-duplex-based IEEE 802.15.4 and IEEE 802.11," *IEEE Trans. Ind. Inform.*, vol. 14, no. 12, pp. 5389–5399, Dec. 2018.

[37] E. Ahmed and A. M. Eltawil, "All-digital self-interference cancellation technique for full-duplex systems," *IEEE Trans. Wireless Commun.*, vol. 14, no. 7, pp. 3519–3532, Jul. 2015.

[38] S. Mori, K. Mizutani, and H. Harada, "In-band full-duplex-applicable area expansion by inter-user interference reduction using successive interference cancellation," *IEICE Trans. Commun.*, vol. E105-B, no. 2, pp. 168–1786, Feb. 2022.

[39] H. Mehrpouyan and S. D. Blostein, "ARMA synthesis of fading channels," *IEEE Trans. Wireless Commun.*, vol. 7, no. 8, pp. 2846–2850, Aug. 2008.

[40] ARIB, "920 MHz-band telemeter, telecontrol and data transmission radio equipment: ARIB STD-T108," Version 1.5, Mar. 2023. Accessed: Jun. 13, 2023. [Online]. Available: https://www.arib.or.jp/english/html/overview/doc/5-STD-T108v1_5-E1.pdf

YUDAI MORIKAWA received the B.E. degree in electric and electrical engineering from Kyoto University, Kyoto, Japan, in 2021, where he is currently working toward the M.I. degree with the Graduate School of Informatics. His research interests include physical layer technologies in in-band full duplex systems (IBFD). He was the recipient of the IEEE VTS Tokyo/Japan Chapter Student Encouragement Award from the IEEE VTS Tokyo/Japan Chapter in 2021.

KEIICHI MIZUTANI (Member, IEEE) received the B.E. degree in engineering from Osaka Prefecture University, Sakai, Japan, in 2007, and the M.E. and Ph.D. degrees in engineering from the Tokyo Institute of Technology, Tokyo, Japan, in 2009 and 2012, respectively. He is currently an Associate Professor with the Graduate School of Informatics, Kyoto University, Kyoto, Japan. In 2010, he was an invited Researcher with Fraunhofer Heinrich Hertz Institute, Berlin, Germany. From 2012 to 2014, he was a Researcher with the National Institute of Information and Communications Technology (NICT), Tokyo. From 2014 to 2021, he was an Assistant Professor with the Graduate School of Informatics, Kyoto University. From 2021 to 2022, he was an Associate Professor with the School of Platforms, Kyoto University. His research interests include physical layer technologies in white space communications, dynamic spectrum access, wireless smart utility networks (Wi-SUN), and 4G/5G/6G systems including OFDM, OFDMA, MIMO, multi-hop relay network, and full-duplex cellular systems. Since joining in NICT, he has been involved in IEEE 802 standardization activities, namely 802.11af, 802.15.4m and 802.22b. He was the recipient of the Special Technical Awards from IEICE SR technical committee in 2009 and 2017, Best Paper Award from IEICE SR technical committee in 2010 and 2020, Young Researcher's Award from IEICE SRW Technical Committee in 2016, Best Paper Award from WPMC2017 and WPMC2020, and Best Paper Presentation Award (1st Place) from IEEE WF-IoT 2020.

HIROSHI HARADA (Member, IEEE) is currently a Professor with the Graduate School of Informatics, Kyoto University, Kyoto, Japan, and an Executive Research Director of the Wireless Networks Research Center, National Institute of Information and Communications Technology (NICT), Tokyo, Japan. He joined the Communications Research Laboratory, Ministry of Posts and Communications, in 1995 (currently, NICT). In 1995, he researched software radio, cognitive radio, dynamic spectrum access network, wireless smart ubiquitous network (Wi-SUN), and broadband wireless access systems. He has authored the book entitled Simulation and Software Radio for Mobile Communications (Artech House, 2002). He also has joined many standardization committees and forums in the United States as well as in Japan and fulfilled important roles for them, especially IEEE 1900 and IEEE 802. He was the Chair of IEEE DySpan Standards Committee and Vice Chair of IEEE 802.15.4g, IEEE 802.15.4m, IEEE 1900.4, and TIA TR-51. He was the board of directors of IEEE communication society standards board, SDR forum, DSA alliance, and WhiteSpace alliance. He is the Co-founder of Wi-SUN alliance. From 2012 to 2019, he was the Chairman of the board. He is currently the Vice Chair of IEEE 2857, IEEE 802.15.4aa and Wi-SUN alliance. He moreover was the Chair of the IEICE Technical Committee on Software Radio and Chair of Public Broadband Mobile Communication Development Committee, ARIB. He is also involved in many other activities related to telecommunications. He was the recipient of the achievement awards in 2006 and 2018, respectively, and the achievement awards of ARIB in 2009 and 2018, respectively, on the topic of research and development on software radio, cognitive radio, and Wi-SUN. In 2009, he was a Fellow of IEICE.